Supporting Information

Barnard et al. 10.1073/pnas.1216407109

SI Text

Numerical Model. The carbon nanotube (CNT) is modeled as a discretized finite element structure—a linear chain of masses with tensional and flexural springs joining neighboring masses. For N masses, this yields a system of $3N$ second-order or $6N$ first-order differential equations describing the time dynamics in 3D of all masses. For a given single-wall CNT, the tube's linear mass density μ is related to graphene's 2D mass density $\sigma = 7.67\times10^{-25}\frac{kg}{m^2}$ by $\mu = \pi d\sigma$. Thus, for a given discretization length Δx, this gives a mass of $m = \mu\Delta x = \pi\sigma d\Delta x$. The linear spring constant between masses is then related to the rigidity K by $k_{stretch} = \frac{K}{\Delta x}$. Finally, there is a torque applied proportional to the angle between two adjoining segments related to the bending rigidity κ: $|\tau| = \frac{\kappa}{\Delta x}|\theta|$. With these values, the initial conditions are solved for by numerically approaching a steady-state solution using the Newton–Raphson method to find the zero of the $3N\times 3N$ force constant matrix $\frac{\partial^2 U}{\partial x_n \partial x_m}$.

The resonance modes are thermalized by including a global damping coefficient γ, and applying stochastic momentum kicks to each mass in all directions, with amplitudes set by γ, the temperature T, and the time-step size Δt:

$$\frac{\Delta p}{\Delta t} = \sqrt{\frac{6\pi\sigma d\gamma k_B T}{\Delta x \Delta t}} U(-1,1), \qquad [S1]$$

where $U(-1, 1)$ denotes a uniform random distribution in the range from -1 to 1. In all reported data, $\gamma \le 250$ kHz, which is smaller than all observed line widths, and thus not the dominant source of apparent broadening. With the equations of motion set, time series are computed using the fourth-order Runge–Kutta method.

***Q* vs. ϵ_0.** The Q of a CNT resonator changes with ϵ_0 because it influences the coupling between resonance modes, both by modifying thermal amplitudes and by changing equilibrium geometry. Under tension, the resonance widths narrow with increasing tension, because all modes decrease their thermal amplitudes and thus tend to couple less strongly among one another. In addition to this effect, the bare frequencies increase as $\sim\epsilon_0^{\frac{1}{2}}$, leading to an additional increase in Q with ϵ_0. Eq. **2** accounts for these two effects, and when expressed with the full dependence on ϵ we see

$$Q \sim \epsilon^{\frac{7}{4}}. \qquad [S2]$$

Solving for Eq. **2** at 100 K over a range of positive strain gives the blue line shown in Fig. S1*A*, which is plotted along with simulation results.

Under compression, the bare frequencies of most modes do not vary significantly with strain; however, the coupling between resonance modes goes inversely with $|\epsilon|$ as seen in the derivation of Eq. **4** in Eqs. **S30–S37**. Eq. **4**, computed over a range of negative strain, gives the blue line in Fig. S1*B*, which is similarly plotted along with simulation results.

Calculation of *Q* for Tensioned NT. The tension of the resonator is affected quadratically by the deflection of each resonance mode, thus the time-averaged tension is nontrivially modified by the rms amplitude of each resonance mode:

$$\langle\epsilon\rangle \approx \epsilon_0 + \sum_{n,a} \beta_{na}\frac{\langle a_n^2\rangle}{2L^2}. \qquad [S3]$$

Assuming Maxwell–Boltzmann statistics, we can substitute for the rms amplitude of the n^{th} mode:

$$\langle a_n^2\rangle = \frac{k_B T}{k_{na}} \approx \frac{k_B T}{\beta_{na}\frac{K\epsilon}{L} + \alpha_{na}\frac{\kappa}{L^3}}, \qquad [S4]$$

where k_{na} is the effective spring constant and $\alpha_{na} \equiv \int_0^1 \xi_{na}''(x)^2 dx$ parameterizes the bending associated with the n^{th} eigenmode. Combining Eqs. **S3** and **S4** yields

$$\langle\epsilon\rangle \approx \epsilon_0 + \frac{k_B T}{2NL}\sum_{n,a}\frac{1}{1+\frac{\alpha_{na}}{\beta_{na}}\frac{\kappa}{NL^2}}. \qquad [S5]$$

In the case of a tensioned string, $\beta_{na} \sim n^2\pi^2$ and $\alpha_{na} \sim n^4\pi^4$. Therefore, in the high-tension limit, the argument in the series in Eq. **S5** is of order unity for small n, which leads to the conclusion that all low-n modes contribute equally to the shifts in strain. Consequently, we aim to carry out this sum, and relate it to the total number of fluctuating degrees of freedom that contribute to the tension shift. In the high-tension limit, the series argument is slowly varying, so it can be approximated by an integral:

$$\sum_{n,a}\frac{1}{1+\frac{\alpha_{na}}{\beta_{na}}\frac{\kappa}{NL^2}} \approx 2\int_0^\infty \frac{1}{1+\frac{n^2\pi^2\kappa}{NL^2}}dn, \qquad [S6]$$

where the 2 is due to the sum over the a index. Solving the integral yields

$$2\int_0^\infty \frac{1}{1+\frac{n^2\pi^2\kappa}{NL^2}}dn = \frac{2}{\pi}\sqrt{\frac{NL^2}{\kappa}}\int_0^\infty \frac{1}{1+n'^2}dn' = \sqrt{\frac{NL^2}{\kappa}}, \qquad [S7]$$

which we define as n_f, the apparent number of fluctuating degrees of freedom affecting the tension. With n_f calculated, we have a solution for the strain shift:

$$\overline{\Delta\epsilon} = \langle\epsilon\rangle - \epsilon_0 \approx \frac{k_B T}{2NL}n_f = \frac{L}{2n_f\ell_p}. \qquad [S8]$$

Because n_f is dependent on ϵ, the above equation needs to be solved self-consistently, which can be accomplished by iterative numerical analysis. The negative curvature shown in Fig. 2*C* is a result of this modification of n_f.

Next, we calculate the fluctuations in ϵ to determine the expected spectral linewidth for a given mode, and thus determine the expected Q. We start by relating the variance of the strain to the calculable variance of squared amplitudes of all resonance modes:

$$\sigma_\epsilon^2 = \sum_{n,a}\left|\frac{\partial\epsilon}{\partial a_n^2}\right|^2\sigma_{a_n^2}^2 = \sum_{n,a}\frac{\beta_{na}^2}{4L^4}\left(\overline{a_n^4} - \overline{a_n^2}^2\right). \qquad [S9]$$

Due to Maxwell–Boltzmann statistics, we know the probability distribution for the squared amplitudes of the resonance modes, and thus can calculate and substitute for $\overline{a_n^4}$ and $\overline{a_n^2}$:

$$p(a_n^2)da_n^2 = \frac{k_{na}}{k_BT}e^{\frac{-k_{na}a_n^2}{k_BT}}da_n^2 \Rightarrow \overline{a_n^2} = \frac{k_BT}{k_{na}}; \overline{a_n^4} = 2\left(\frac{k_BT}{k_{na}}\right)^2. \quad [S10]$$

As above, we can carry out the series to calculate the strain variance:

$$\sigma_\epsilon^2 = \sum_{n,a}\frac{\beta_{na}^2}{4L^4}\left(\frac{k_BT}{k_{na}}\right)^2 = \left(\frac{k_BT}{2NL}\right)^2\sum_{n,a}\frac{1}{1+\left(\frac{\alpha_{na}}{\beta_{na}}\frac{\kappa}{NL^2}\right)^2} \quad [S11]$$

$$\sum_{n,a}\frac{1}{1+\left(\frac{\alpha_{na}}{\beta_{na}}\frac{\kappa}{NL^2}\right)^2} \approx \frac{2}{\pi}\sqrt{\frac{NL^2}{\kappa}}\int_0^\infty\left(\frac{1}{\left(1+n'^2\right)^2}dn'\right) = \frac{1}{2}\sqrt{\frac{NL^2}{\kappa}} \quad [S12]$$

$$\sigma_\epsilon^2 = \frac{1}{8}\left(\frac{k_BT}{NL}\right)^2\sqrt{\frac{NL^2}{\kappa}} = \frac{L^2}{8n_f^3\ell_p^2}. \quad [S13]$$

The strain fluctuations directly lead to frequency fluctuations, and thus affect the resonance width. Consequently, we are able to calculate the expected quality factor:

$$Q^{-1} = \frac{\delta f_{FWHM}}{f} = \sqrt{8\ \ln(2)}\ \frac{\sigma_f}{f} = \sqrt{2\ \ln(2)}\ \frac{\sigma_\epsilon}{\epsilon}. \quad [S14]$$

The $\sqrt{8\ln(2)}$ factor relates the variance of a Gaussian distribution to its FWHM. Although it is not regularly assumed that a resonance peak will have a Gaussian profile, the above theory implies this, and the simulated power spectral density displays mostly Gaussian peaks with Lorentzian tails, as seen in Fig. 2. With this we predict for the inverse quality factor for tensioned nanotubes:

$$Q^{-1} = \frac{\sqrt{\ln 2}}{2}\frac{L}{n_f^{\frac{3}{2}}\epsilon\ell_p}. \quad [S15]$$

Derivation of Eq. 3. The length constraint requires that the deflection of an out-of-plane mode is accompanied by an in-plane deflection. In our simplifying assumption, we assert that the in-plane deflection is in the shape of the static buckling. This deflection amounts to a driving force distributed among all in-plane modes. Focusing on a single pair of in- and out-of-plane modes, we can write down the Lagrangian:

$$L = \frac{1}{2}m\dot{z}_{ip}^2 + \frac{1}{2}m\dot{x}_{op}^2 - \frac{1}{2}k_{ip}\left(z_{ip} - \frac{\eta}{L}\beta_{op}x_{op}^2\right)^2 - \frac{1}{2}k_{op}x_{op}^2. \quad [S16]$$

Solving for the equations of motion, we get

$$m\ddot{z}_{ip} = -k_{ip}\left(z_{ip} - \frac{\eta}{L}x_{op}^2\right) \quad [S17]$$

$$m\ddot{x}_{op} = -k_{op}x_{op} - 2k_{ip}\frac{\eta}{L}x_{op}\left(z_{ip} - \frac{\eta}{L}x_{op}^2\right). \quad [S18]$$

Eqs. **S17** and **S18** are nonlinearly coupled equations that we now seek to simplify, because our main goal is to understand how the resonance frequencies shift based on the amplitudes of the relevant modes, as opposed to the detailed phase relationships. Consequently, we will recast the coupling in terms of a mean-field interaction matrix. Because the coupling is quadratic in x_{op}, we express Eq. **S17** in terms of its apparent in-plane deflection:

$$z_{op} \equiv \frac{\eta}{L}\beta_{op}x_{op}^2. \quad [S19]$$

To substitute into Eq. **S18**, we rewrite Eq. **S19** in terms of x_{op} and compute the second derivative, respectively,

$$x_{op} = \sqrt{\frac{z_{ip}L}{\eta\beta_{op}}} \quad [S20]$$

$$\ddot{x}_{op} = -\frac{1}{4}\frac{\left(\dot{z}_{op}\right)^2}{z_{op}^2} + \frac{1}{2}\frac{\ddot{z}_{op}}{z_{op}}, \quad [S21]$$

which gives

$$m\left(2\ddot{z}_{op} - \frac{\left(\dot{z}_{op}\right)^2}{z_{op}}\right) = -4k_{op}z_{op} + 8k_{ip}\frac{\eta}{L}z_{op}\left(z_{ip} - z_{op}\right). \quad [S22]$$

The solution to Eq. **S22** in the absence of coupling is

$$z_{op} = \bar{z}[\cos(2\omega t + \phi) + 1], \quad [S23]$$

where $\omega = \sqrt{\frac{k_{op}}{m}}$. In the weak coupling limit, we can assume that z_{op} retains this approximate functional form, whereas the frequency may be perturbed by the interaction term. With this approximation in mind, we calculate all of the relevant terms seen in Eq. **S22**:

$$\frac{\left(\dot{z}_{op}\right)^2}{z_{op}} = 4\omega^2\bar{z}(1 - \cos(2\omega t + \phi)) \quad [S24]$$

$$\ddot{z}_{op} = -4\omega^2\bar{z}\cos(2\omega t + \phi). \quad [S25]$$

The first effect we solve for is due to the term in Eq. **S22** containing z_{op}^2, which originates from the x_{op}^3 term in Eq. **S18**. Neglecting the $z_{op}z_{ip}$ term, and dropping all oscillating terms, we solve for the modified frequency:

$$\omega^2 = \omega_{op}^2 + 3\bar{z}\omega_{ip}^2\frac{\eta\beta_{op}}{L}. \quad [S26]$$

Next, we solve for the effect due to the $z_{op}z_{ip}$ term in Eq. **S22**. Here we substitute $z_{ip} = \bar{z}_{ip}cos(\omega_{ip}t + \theta)$, and assuming $|2\omega_{op} - \omega_{ip}| \ll |2\omega_{op} + \omega_{ip}|$, we retain only terms close in frequency to $2\omega_{op}$ and get

$$2\ddot{z}_{op} - \frac{\left(\dot{z}_{op}\right)^2}{z_{op}} = -4\omega_{op}^2z_{op} + \left[8\omega_{ip}^2\frac{\eta\beta_{op}}{L}\bar{z}_{op}\right]z_{ip}. \quad [S27]$$

Combining the conclusions from Eqs. **S26** and **S27**, substituting for $\bar{z}_{op} = 2\frac{\eta\beta_{op}}{L}\langle x^2\rangle$ we rewrite Eqs. **S17** and **S22** to obtain linearized equations of motion:

$$m\ddot{z}_{ip} = -k_{ip}z_{ip} + k_{ip}z_{op} \quad \text{[S28]}$$

$$m\ddot{z}_{op} = \left[16k_{ip}\left(\frac{\eta\beta_{op}}{L}\right)^2\langle x^2\rangle\right]z_{ip} - \left[4k_{op} + 24k_{ip}\left(\frac{\eta\beta_{op}}{L}\right)^2\langle x^2\rangle\right]z_{op}. \quad \text{[S29]}$$

Finally, we express the coupled equations in matrix form, symmetrizing the off-diagonal elements by taking the geometric mean, so that the eigenvectors are in the basis of the original, uncoupled solutions; this results in Eq. **3** in the main text.

Calculation of *Q* for Buckled NT. Solving for the quality factor of the buckled NT follows an analogous procedure to that in the tensioned NT, where Q is obtained by averaging over a statistical distribution of frequencies. Eq. **3** can be solved for eigenfrequencies that are dependent on the amplitude of the out-of-plane mode:

$$\omega_{\pm}^2 = \frac{\omega_{ip}^2\left(1+4\alpha^2(T)\right)+4\omega_{op}^2}{2} \pm \frac{\left|\omega_{ip}^2\left(1-4\alpha^2(T)\right)-4\omega_{op}^2\right|}{2}\sqrt{1+\frac{\alpha^2(T)\omega_{ip}^4}{\left(\omega_{ip}^2(1-4\alpha^2(T))-4\omega_{op}^2\right)^2}}. \quad \text{[S30]}$$

In the weak coupling limit, the lower eigenfrequency in Eq. **S30** (which corresponds to dominant the in-plane motion) reduces to

$$\omega_- \approx \omega_{ip}\left(1-\frac{\alpha^2(T)}{8}\frac{1}{\left(\frac{2\omega_{op}}{\omega_{ip}}\right)^2-1}\right). \quad \text{[S31]}$$

In the low-tension limit, the ratio of the lowest in-plane and out-of-plane flexural modes for a Euler-buckled beam is a fixed value, giving

$$\frac{1}{\left(\frac{2\omega_{op}}{\omega_{ip}}\right)^2-1} = 2.4. \quad \text{[S32]}$$

Finally, $\alpha^2(T) \propto \langle x_{op}^2\rangle$, so we can solve for

$$\sigma_f = \left|\frac{\partial f}{\partial x_{op}^2}\right|\sigma_{x_{op}^2} \quad \text{[S33]}$$

$$\sigma_f = \frac{1}{2\pi}\left|\frac{\partial\omega_-}{\partial x_{op}^2}\right|\sigma_{x_{op}^2} = \frac{\omega_{ip}}{2\pi}0.3\frac{64\pi^4\eta^2}{L^2}\frac{L^3k_BT}{16\pi^4\kappa} \quad \text{[S34]}$$

$$\frac{\sigma_f}{f} = 1.2\eta^2\frac{L}{\ell_p}. \quad \text{[S35]}$$

Carrying out the appropriate inner products gives $\eta^2 = \frac{0.05}{|\epsilon|}$, which when substituted into the above equation gives

$$\frac{\sigma_f}{f} = 0.06\frac{L}{|\epsilon|\ell_p}. \quad \text{[S36]}$$

Here, the relationship between the variance and FWHM of the distribution is not set by a Gaussian distribution as in Eq. **S2**. The line shape is notably skewed, and according to the simplified approach outlined above, the line shape is represented by an exponential probability function, which gives $0.69\sigma_f \sim \delta f_{FWHM}$, and this in turn gives

$$Q^{-1} \approx 0.04\frac{L}{|\epsilon|\ell_p}. \quad \text{[S37]}$$

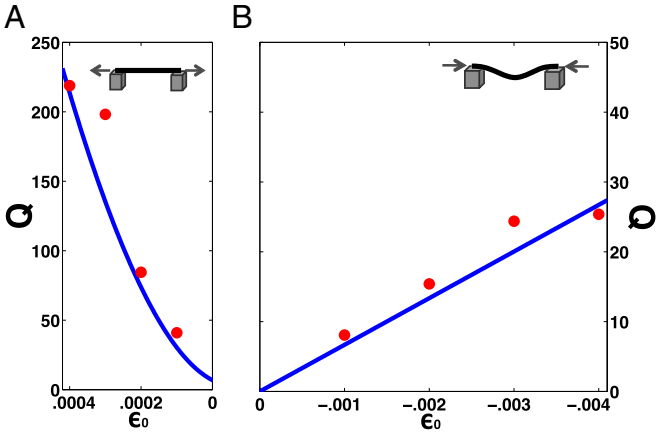

Fig. S1. Q vs. ϵ_0 at 100 K. Eqs. **2** and **4** are shown as blue lines in *A* and *B*, respectively. Corresponding simulation results are shown as red circles.